UvA-DARE (Digital Academic Repository)

Radio and X-ray monitoring of the accreting millisecond X-ray pulsar IGR J17591-2342 in outburst

Gusinskaia, N. V.; Russell, T.D.; Hessels, J.W.T.; Bogdanov, S.; Degenaar, N.; Deller, A.T.; van den Eijnden, J.; Jaodand, A.D.; Miller-Jones, J.C.A.; Wijnands, R.

Link to publication

Radio and X-ray monitoring of the accreting millisecond X-ray pulsar IGR J17591−2342 in outburst

N. V. Gusinskaia [1,2]★ T. D. Russell [1] J. W. T. Hessels,[1,2] S. Bogdanov,[3] N. Degenaar,[1] A. T. Deller [4] J. van den Eijnden [1] A. D. Jaodand,[5] J. C. A. Miller-Jones [6] and R. Wijnands[1]

[1]*Anton Pannekoek Institute for Astronomy, University of Amsterdam, Science Park 904, NL-1098 XH Amsterdam, the Netherlands*
[2]*ASTRON, the Netherlands Institute for Radio Astronomy, Postbus 2, NL-7990 AA Dwingeloo, the Netherlands*
[3]*Columbia Astrophysics Laboratory, Columbia University, 550 West 120th Street, New York, NY 10027, USA*
[4]*Centre for Astrophysics and Supercomputing, Swinburne University of Technology, P.O. Box 218, Hawthorn, VIC 3122, Australia*
[5]*Cahill Center for Astrophysics, 1216 E. California Blvd, California Institute of Technology, Pasadena, CA 91125, USA*
[6]*International Centre for Radio Astronomy Research, Curtin University. GPO Box U1987, Perth, WA 6845, Australia*

ABSTRACT

IGR J17591−2342 is a new accreting millisecond X-ray pulsar that was recently discovered in outburst in 2018. Early observations revealed that the source's radio emission is brighter than that of any other known neutron star low-mass X-ray binary (NS–LMXB) at comparable X-ray luminosity, and assuming its likely $\gtrsim 6$ kpc distance. It is comparably radio bright to black hole LMXBs at similar X-ray luminosities. In this work, we present the results of our extensive radio and X-ray monitoring campaign of the 2018 outburst of IGR J17591−2342. In total, we collected 10 quasi-simultaneous radio (VLA, ATCA) and X-ray (*Swift*–XRT) observations, which make IGR J17591−2342 one of the best-sampled NS–LMXBs. We use these to fit a power-law correlation index $\beta = 0.37^{+0.42}_{-0.40}$ between observed radio and X-ray luminosities ($L_\mathrm{R} \propto L_\mathrm{X}{}^{\beta}$). However, our monitoring revealed a large scatter in IGR J17591−2342's radio luminosity (at a similar X-ray luminosity, $L_\mathrm{X} \sim 10^{36}$ erg s^{-1}, and spectral state), with $L_\mathrm{R} \sim 4 \times 10^{29}$ erg s^{-1} during the first three reported observations, and up to a factor of 4 lower L_R during later radio observations. None the less, the average radio luminosity of IGR J17591−2342 is still one of the highest among NS–LMXBs, and we discuss possible reasons for the wide range of radio luminosities observed in such systems during outburst. We found no evidence for radio pulsations from IGR J17591−2342 in our Green Bank Telescope observations performed shortly after the source returned to quiescence. None the less, we cannot rule out that IGR J17591−2342 becomes a radio millisecond pulsar during quiescence.

Key words: stars: neutron – X-rays: binaries.

1 INTRODUCTION

Low-mass X-ray binaries (LMXBs; Lewin, van Paradijs & van den Heuvel 1997) are systems in which a black hole (BH) or neutron star (NS) primary accretes material from a low-mass companion star that overflows its Roche lobe and forms of an accretion disc around the primary. Quasi-simultaneous radio (L_R) and X-ray (L_X) luminosity measurements of such systems can help probe the interplay between accretion inflow: X-rays, which probe the innermost parts of the accretion disc and matter transfer onto the primary in the case of

NSs; and outflow: flat[1] or inverted spectrum radio emission from a partially self-absorbed, collimated jet[2] (e.g. Migliari & Fender 2006; Gallo, Miller & Fender 2012; Corbel et al. 2013).

In the last few years, new and upgraded radio telescopes – like the Karl G. Jansky Very Large Array (VLA), the Australia Telescope Compact Array (ATCA), and MeerKAT – coupled with flexible X-ray observatories such as the Neil Gehrels Swift X-ray Telescope (*Swift*–XRT), have provided the sensitivity and rapid

---

[1]Spectral index $\alpha \sim 0$, where the flux density S_ν at frequency ν scales as $S_\nu \propto \nu^{\alpha}$.
[2]Although not all observed radio emission is consistent with coming from a compact jet (Bogdanov et al. 2018).

★ E-mail: N.Gusinskaia@uva.nl

response required to probe a steadily increasing number of known Galactic NS–LMXBs. This includes accreting millisecond X-ray pulsars (AMXPs; Tudor et al. 2017), where the accretion flow is channelled by the NS's magnetic field (producing coherent X-ray pulsations: e.g. Wijnands & van der Klis 1998; see Patruno & Watts 2012 for a review), as well as non-pulsing NS–LMXBs – both of which have been observed in the hard and soft X-ray spectral states (e.g. Gusinskaia et al. 2017).

NS–LMXBs have been observed during their bright (X-ray luminosity $L_X \sim 10^{36-38}$ erg s^{-1}) accretion outbursts (e.g. Migliari & Fender 2006), and as they fade back to quiescence. This has allowed the L_R–L_X relationship in the hard X-ray state to be studied for both individual systems (e.g. Migliari et al. 2003; Tudose et al. 2009; Tetarenko et al. 2016) as well as statistically for the population as a whole (e.g. Gallo, Degenaar & van den Eijnden 2018). Previous studies have modelled the radio–X-ray luminosity scaling in the simplistic form $L_R \propto L_X{}^\beta$. Recent work by Gallo et al. (2018) finds $\beta = 0.44^{+0.05}_{-0.04}$ and $\beta = 0.59 \pm 0.02$ for the NS– and BH–LMXB populations, respectively. Gallo et al. (2018) also found that NS–LMXBs are, on average, $\sim$20 times less radio luminous compared to BH–LMXBs at the same L_X.

Overall, radio observations during the hard X-ray state are consistent with the presence of a compact, partially self-absorbed jet during outburst (Blandford & Znajek 1977; Blandford & Payne 1982). However, both NS–LMXB and BH–LMXB show a wide range of L_R for comparable L_X, as well as roughly a 2 order-of-magnitude spread in average L_R between systems. Furthermore, individual systems show different power-law slopes compared to the global averages (Tudor et al. 2017; Gusinskaia et al. 2019). There is currently no clear physical picture explaining this observed diversity, but perhaps it is unsurprising given that NS–LMXBs have a range of NS spin rate, magnetic field, and magnetospheric inclination with respect to the disc. In the case of AMXPs, Tudor et al. (2017) question whether it is even appropriate to fit a single L_R–L_X correlation over a broad luminosity range ($>$1 dex, i.e. an order of magnitude) because these systems show very large scatter. The same could be said for NS–LMXBs in general, where to date there is no demonstrated tight power-law correlation for individual systems over a large ($>$2 dex) luminosity range (Gusinskaia et al. 2019).

AMXPs like SAX J1808.4−3658 directly demonstrated that NSs with millisecond spin periods exist in accreting systems (Wijnands & van der Klis 1998), thereby providing strong observational support for the recycling scenario in which radio millisecond pulsars (MSPs) are formed via the transfer of mass and angular momentum in such systems (Alpar et al. 1982; Radhakrishnan & Srinivasan 1982). This scenario has been further demonstrated by the relatively recently identified class of transitional millisecond pulsars (tMSPs), which switch on multiyear time-scales between radio pulsar and accretion-disc states (e.g. Archibald et al. 2009; Papitto et al. 2013; Stappers et al. 2014). These have been observed using high-sensitivity multiwavelength campaigns during their prolonged low-luminosity disc states ($L_X \sim 10^{32-34}$ erg s^{-1}; one of the tMSPs, M28I, has shown a full AMXP-like outburst). While their bright (compared to other NS–LMXBs) and rapidly variable radio emission was initially ascribed to a compact, partially self-absorbed synchrotron jet (Deller et al. 2015), the discovery of an anticorrelation between radio and X-ray luminosity in strictly simultaneous observations suggests a different physical mechanism (Bogdanov et al. 2018). This is supported by recent multiwavelength observations, which suggest rapid ejection due to a pulsar wind (Papitto et al. 2019; Jaodand et al., in preparation).

Despite the great increase in NS–LMXB L_R–L_X measurements in recent times, additional observations – both of new systems, as well as higher cadence and/or strictly simultaneous radio – X-ray observations of previously observed systems – are needed to identify possible correlations between radio brightness and system parameters like the orbital inclination, neutron star mass, spin rate, magnetic field strength, and orbital period. For example, van den Eijnden et al. (2018a) detect a faint radio jet from a highly magnetized ($B > 10^{12}$ G), slowly spinning NS accreting at a rate above the theoretical Eddington limit. They argue that the magnetic field strength of the NS could have a significant role in dictating the radio brightness, but whether this is also applicable to lower magnetic field systems is unknown. At the same time, recent numerical simulations are investigating the role of the NS magnetic field (Parfrey, Spitkovsky & Beloborodov 2016, 2017; Parfrey & Tchekhovskoy 2017).
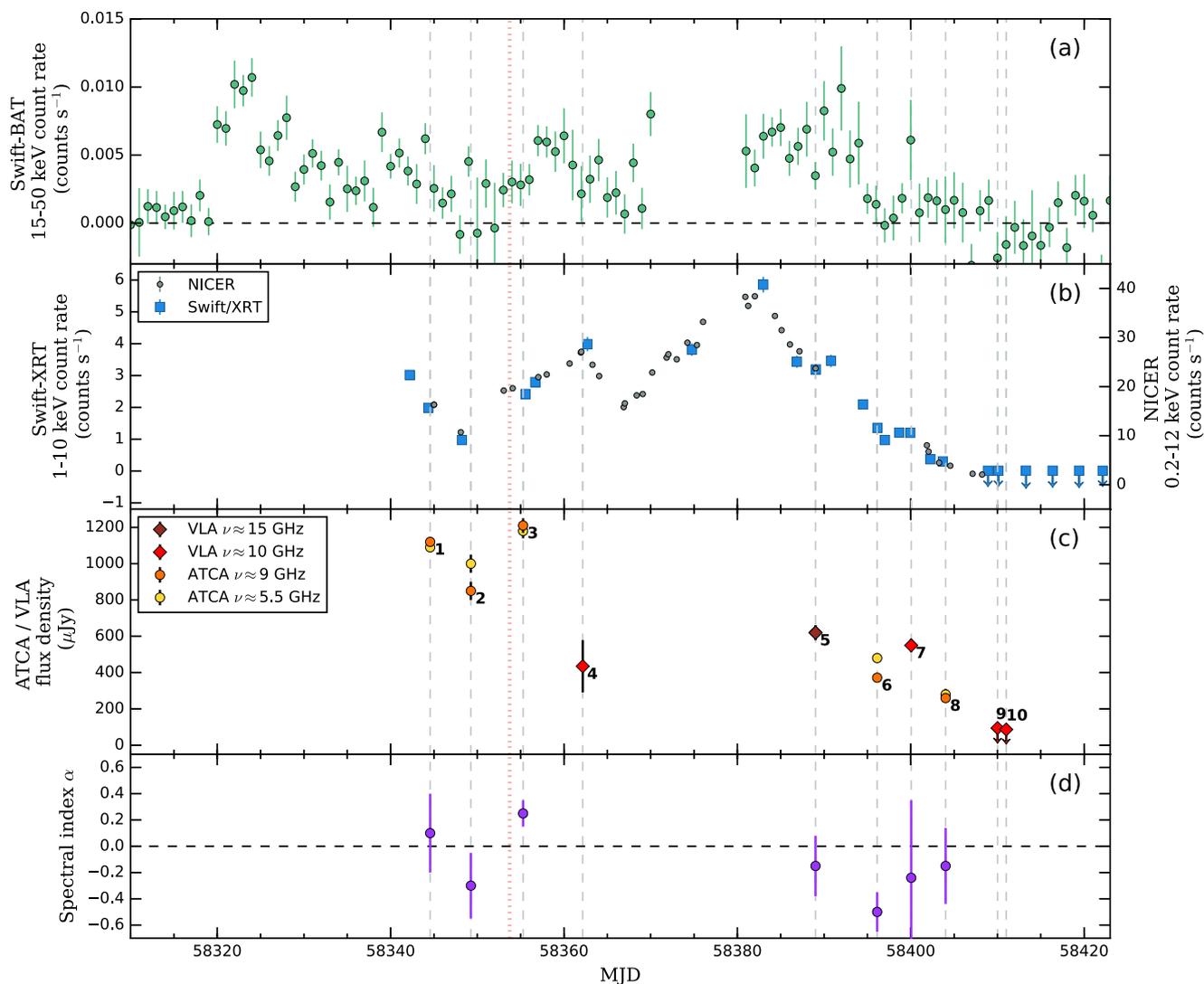
1.1 IGR J17591−2342

On 2018 August 10−11, during its continuing survey of the Galactic bulge and centre, the International Gamma-Ray Astrophysics Laboratory (*INTEGRAL*) X-ray and gamma-ray telescope discovered a new transient, IGR J17591−2342 (Ducci et al. 2018). The high absorption seen in the X-ray spectrum (Bozzo et al. 2018; Nowak et al. 2018) suggested that this source is likely roughly at the distance of the Galactic centre ($\sim$8 kpc). Nowak et al. (2019) further investigate and discuss the source distance, and conclude that it is very likely at the distance of the Galactic bulge or beyond ($>$6 kpc). Russell & Lewis (2018) could not identify an optical counterpart, but Shaw, Degenaar & Heinke (2018) detected an associated transient near-infrared source.

Initial radio observations using ATCA measured a high-flux density, typical of that seen in BH–LMXBs when the X-ray luminosity is $\sim$10^{36} erg s^{-1} (Russell et al. 2018a, b). However, timing analysis of follow-up Nuclear Spectroscopic Telescope Array (*NuSTAR*) and Neutron Star Interior Composition Explorer (*NICER*) observations revealed 527-Hz coherent X-ray pulsations, showing that IGR J17591−2342 was an AMXP in outburst (Ferrigno et al. 2018; Sanna et al. 2018). Other properties of the source were also similar to those typically seen for other AMXPs (and NS–LMXBs) in outburst, e.g. a relatively low-peak X-ray luminosity ($L_X \sim 10^{36}$ erg s^{-1}) and hard spectrum (photon index $\Gamma \sim 2$).

The outburst displayed a light curve with multiple brightness peaks over the course of its approximately 3-month duration (Fig. 1). Based on archival data from the *Swift*–Burst Alert Telescope (*Swift*–BAT), Krimm et al. (2018) reported that the outburst had actually started on roughly July 22 (about 3 weeks prior to the discovery by *INTEGRAL*), peaked on July 25 and decayed thereafter. As such, the initial radio observations of Russell et al. (2018a) were performed close in time, but weeks after the first bright peak of the outburst (Fig. 1), and did not sample the later X-ray bright peaks that were observed (Kuiper et al. 2018; Ray et al. 2018; Sanchez-Fernandez et al. 2018).

Nowak et al. (2019) presented high-resolution spectroscopy using the *Chandra X-ray Observatory*, performed during the start of the second peak of the outburst (see the red-dotted vertical line in Fig. 1) and demonstrated evidence for an outflowing wind in IGR J17591−2342. The AMXP SAX J1808.4−3658 also showed evidence for a wind (Pinto et al. 2014). Such X-ray winds are usually observed during the soft X-ray states of LMXBs, in which the jet is typically quenched (Miller et al. 2006; Neilsen & Lee 2009;

Figure 1. X-ray and radio light-curves during the 2018 outburst of IGR J17591−2342. The downward pointing arrows indicate 3σ upper limits in all cases. Panel (a): *Swift*–BAT (15–50 keV) daily X-ray light curve. Panel (b): the blue squares represent the *Swift*–XRT (1–10 keV) X-ray light curve (using the left-hand axis). The grey circles represent the *NICER* (0.2–12 keV) X-ray light curve (using the right-hand axis). Panel (c): Radio light curve. The circles and the diamonds represent ATCA and VLA observations, respectively; their colour shade represents the frequency. Panel (d): Inferred radio spectral index α, where $S_\nu \propto \nu^\alpha$. The vertical grey-dashed lines indicate the epochs of radio observations. The vertical red-dotted line indicates the *Chandra* observation epoch in which a wind was detected (Nowak et al. 2019).

Ponti et al. 2012). However, Homan et al. (2016) found that for high-luminosity NSs (Z-sources), high-velocity winds are observed during the hardest spectral state, where radio jet emission is the brightest.

X-ray timing observations provided a precise orbital ephemeris and showed that IGR J17591−2342 has an orbital period $P_b =$ 8.8 h and a minimum companion mass $0.42\,M_\odot$ (Sanna et al. 2018). This, along with its relatively high spin rate, makes IGR J17591−2342 quite similar to the well-established tMSP systems PSR J1023 + 0038 (Archibald et al. 2009), PSR J1824−2452I (Papitto et al. 2013), and PSR J1227−4853 (Bassa et al. 2014) – which are all eclipsing radio MSPs with relatively high-mass ($>0.2\,M_\odot$) companions (such systems are termed 'redbacks', Roberts 2013). Overall, IGR J17591−2342 is a possible tMSP candidate (although the observation of more tMSP-like phenomenology would strengthen the case), and

might become a rotation-powered radio pulsar during quiescence.

In this paper, we present quasi-simultaneous radio–X-ray observations that span IGR J17591−2342's 2018 outburst from shortly after its discovery by *INTEGRAL* until it faded into quiescence. This is the largest available radio-monitoring data set; it includes and significantly extends the work of Russell et al. (2018a). We use this to constrain the L_R–L_X correlation for IGR J17591−2342 and to quantitatively compare its average radio luminosity and scatter, in the $4 \times 10^{35}\,\mathrm{erg\,s^{-1}} < L_X < 10^{37}\,\mathrm{erg\,s^{-1}}$ range, with those of AMXPs, non-pulsing NS–LMXBs, and BH–LMXBs. We also present high time-resolution radio observations acquired using the Robert C. Byrd Green Bank Telescope (GBT), with which we search for a radio pulsar signal in the weeks following the outburst – in order to investigate whether IGR J17591−2342 switches on as a radio pulsar in quiescence.

Table 1. VLA and ATCA observations (including those from Russell et al. 2018a, i.e. epochs 1, 2, and 3), together with the corresponding quasi-simultaneous *Swift*–XRT X-ray observations and their spectral properties. All uncertainties are 1σ. A dash is used to mark cases in which no useful constraints could be placed on the radio or X-ray spectrum.

Date 2018	#	Tel.	Radio MJD[b]	S_ν (μJy)	ν (GHz)	Spectral index α	*Swift*–XRT X-ray (1–10 keV) MJD[b]	Obs. ID (PC mode)	Unabsorbed[a] flux $\times 10^{-10}$ (erg s^{-1} cm^{-2})	Photon index	χ^2_ν (dof)
14 Aug	1	ATCA	58344.56	1090 ± 20	5.5	0.1 ± 0.3	58344.027	00010804002	$3.09^{+0.17}_{-0.18}$	1.8 ± 0.2	0.92 (15)
			–	1120 ± 20	9.0	–	–	–	–	–	–
19 Aug	2	ATCA	58349.26	1000 ± 50	5.5	-0.30 ± 0.25	58348.221	00010804004	$1.34^{+0.27}_{-0.11}$	$2.6^{+0.3}_{-0.2}$	0.87 (10)
			–	850 ± 50	9.0	–	–	–	–	–	–
25 Aug	3	ATCA	58355.28	1180 ± 40	5.5	0.25 ± 0.1	58355.527	00010804006	$4.03^{+0.16}_{-0.15}$	2.3 ± 0.1	1.03 (56)
			–	1210 ± 40	9.0	–	–	–	–	–	–
			–	1540 ± 100	17.0	–	–	–	–	–	–
			–	1600 ± 90	19.0	–	–	–	–	–	–
1 Sep	4	VLA	58362.16	435 ± 144	10.0	–	58362.699	00010804009	$5.35^{+0.36}_{-0.29}$	2.4 ± 0.1	0.88 (26)
28 Sep	5	VLA	58389.02	620 ± 40	12.8	-0.15 ± 0.23	58389.058	00010899002	$4.21^{+0.20}_{-0.19}$	2.2 ± 0.1	0.97 (32)
			–	590 ± 20	17.4	–	–	–	–	–	–
5 Oct	6	ATCA	58396.12	480 ± 13	5.5	-0.50 ± 0.15	58396.156	00010804015	$1.54^{+0.06}_{-0.07}$	2.1 ± 0.1	1.11 (32)
			–	372 ± 11	9.0	–	–	–	–	–	–
9 Oct	7	VLA	58400.05	568 ± 48	9.0	-0.24 ± 0.59	58399.941	00010804018	1.26 ± 0.07	2.3 ± 0.1	1.44 (26)
			–	544 ± 37	10.8	–	–	–	–	–	–
13 Oct	8	ATCA	58404.02	280 ± 30	5.5	-0.15 ± 0.29	58403.678	00010804020	$0.54^{+0.11}_{-0.08}$	2.6 ± 0.5	1.4 (5)
			–	260 ± 25	9.0	–	–	–	–	–	–
19 Oct	9	VLA	58410.01	<94.7	10.0	–	58410.103	00010804024	<0.02	2.0[c]	–
20 Oct	10	VLA	58411.01	<86.7	10.0	–	–	–	–	–	–

[a]We used a fixed value of $N_H = 4.4 \pm 0.2 \times 10^{22}$ cm^{-2}, as derived by Nowak et al. (2019).
[b]Mid-point of the observation.
[c]Fixed to determine the upper limit.

2 OBSERVATIONS AND DATA ANALYSIS

2.1 Radio continuum data and analysis

2.1.1 VLA

IGR J17591−2342 was observed with the VLA at five epochs (project ID: 18A-374) on 2018 September 1, 28 and October 9, 19, and 20 (see Table 1). All observations were taken at *X* band (8–12 GHz), except for the second observation (September 28), which was recorded using the *Ku*-band receiver (12–17 GHz). Each observing session had a duration of ~1 h including calibration scans, providing ~30 min of on source time. During all five epochs the array was in D configuration (synthesized beam ~12 arcsec). We used 3C 286 as the flux and bandpass calibrator, and we used J1820−2528 and J1744−3116 as the phase calibrator in the *X*-band and *Ku*-band observations, respectively. All observations were processed using the Common Astronomy Software Application (CASA[3] version 5.4.1; McMullin et al. 2007). During our first three observations, the VLA was still recovering from an extended power outage, and these data had unusual artefacts, which precluded using the standard EVLA-pipeline calibration routine. Instead, all initial calibration and flagging was done manually, following standard calibration procedures within CASA. In order to mitigate effects from diffuse emission in the field, we excluded short baselines (<12 kλ)

from the analysis and performed imaging using the Briggs weighing scheme[4] with robust parameter set to 0.

2.1.2 ATCA

We also observed IGR J17591−2342 using the ATCA on 2018 October 5 and 13 (see Table 1; the typical observing durations were ~4 h), under the project code CX413. The observations were taken at central frequencies of 5.5 and 9 GHz, with 2 GHz of bandwidth at each frequency band, and the array was in 6A configuration. We used PKS 1934–638 for flux and bandpass calibration, while J1752–225 was used for phase calibration. Data were flagged, calibrated, and imaged following standard procedures within CASA. Imaging was carried out using a Briggs robust parameter of 0 to reduce the effects of diffuse emission in the field. In this work, we also use the three ATCA observations of IGR J17591−2342 presented by Russell et al. (2018a).

For all ATCA and VLA radio epochs, we extracted the target flux density by fitting for a point source in the image plane using the imfit task within CASA using the source position reported in Russell et al. (2018a). These radio flux densities, along with spectral indices determined from a least-squares fit to multifrequency measurements, are reported in Table 1 and Fig. 1.

We attempted time-resolved radio analysis to search for intra-observation variability during our VLA and ATCA observations.

[3]https://casa.nrao.edu/

[4]http://www.aoc.nrao.edu/dissertations/dbriggs/

Our observations constrain any brightness variations to within 10 per cent of the average flux density. However, we note that – due to the combination of poor instantaneous UV coverage, a complex field, and low source brightness – our sensitivity to source brightness changes on short time-scales is poor. In particular, for ATCA observations we were unable to search for variability on time-scales shorter than ∼30 min (and on some days only down to 1 h intervals). At the same time, any differences in the source's flux density inferred from 10 to 15-min scans in our VLA observations were dominated by the relatively large uncertainties on the flux density of the source caused by the diffuse emission in the field. Therefore, we cannot constrain possible variability on few minute time-scales (or less), which has been observed in some NS–LMXBs (Bogdanov et al. 2018).

2.2 X-ray data and analysis

In order to obtain the full context of the X-ray luminosity and spectrum during IGR J17591−2342's outburst, we produced light curves using *Swift*–XRT, *Swift*–BAT, and *NICER* observations (Fig. 1). The *Swift*–XRT 1–10 keV light curve was produced using the online *Swift*–XRT data products generator (Evans et al. 2007, 2009; target IDs: 10803, 10804, and 10899). The *Swift*–BAT daily light curve (15–50 keV) was obtained from the *Swift*–BAT transient monitor results provided by the *Swift*–BAT team (Krimm et al. 2013). Lastly, the *NICER* 0.2–12 keV light curve was obtained from the online available event files (observational ID: 12003101). Using the NICERDAS package in HEASOFT (v. 6.24[5]), we filtered out 'hot' Focal Plane Modules (34, 14, and 54) as well as times within Sun, Moon, or South Atlantic Anomaly constraints. We then extracted the light curve using XSELECT.

2.2.1 Swift–*XRT spectral analysis*

To give quasi-simultaneous X-ray flux and spectral context to our radio measurements, we selected 10 *Swift*–XRT observations (target IDs 10804 and 10899) that were performed within 0.6 d of the VLA and ATCA observations (see Table 1 and Fig. 1). All such observations were carried out in the photon counting (PC) mode. Their observation IDs, epochs, and inferred spectral parameters are listed in Table 1.

For this X-ray spectral analysis, we used HEASOFT (v. 6.24). First, we ran the XRT_PIPELINE on each observation for basic data reduction and calibration. Then, we extracted the spectrum for all 10 epochs using XSELECT. The source spectrum was extracted from a 30-pixel-radius circular area, centred on the source position (taken from Russell et al. 2018a), and the background spectrum was extracted from an annular region with 30-pixel inner radius and 60-pixel outer radius, also centred at the source position. Additionally, following Romano et al. (2006), we excluded the 3–5 central pixels of the source region in order to account for pile-up in the case of observations with count rate higher than 1 count per second. To correct for this – and also for known artefacts on the CCD as well as the response of the telescope – we produced the ancillary arf-file using XRTMKARF together with exposure maps for each event and the response file 'swxpc0to12s6_20130101v014.rmf'.

XSPEC (version 12.10.0c; Arnaud 1996) was used to perform the spectral model fit and extract the source flux. We used photons in the 0.4–10 keV range and a simple absorbed power-law model

[5]https://heasarc.gsfc.nasa.gov/docs/software/heasoft/

Table 2. GBT observations.

Date	#	MJD	Duration (s)	Orbital phase[a]
2018-10-28	1	58419.878	2402	0.71–0.79
2018-11-04	2	58426.895	2759	0.85–0.93
2018-11-11	3	58433.886	2653	0.91–0.99

[a]Inferior conjunction is at orbital phase 0.75.

(TBabs * power law in XSPEC) for all observations. We fixed the hydrogen column density parameter in the TBabs model to $N_H = (4.4 \pm 0.2) \times 10^{22}$ cm^{-2} (letting it vary within the errors), which was provided by the extensive analysis of Nowak et al. (2019). We used the additional cflux convolution model to determine the unabsorbed 1–10 keV fluxes and their associated errors for each epoch. The inferred fluxes, photon indices as well as χ_ν^2 values and degrees of freedom (dof) for each observation are listed in Table 1.

2.3 GBT searches for radio pulsations

Subsequent to IGR J17591−2342's accretion outburst, which ended roughly on 2018 October 20, we performed three GBT observations (project code: GBT18B-353), which were spaced weekly on 2018 October 28 and November 4 and 11 (see Table 2). Each observing session was ∼1 h in duration with ∼45 min on source, which is about 8 per cent of the orbital period ($P_b = 8.8$ h; Sanna et al. 2018). It is important to note that 'redback' radio pulsars often exhibit eclipses from intrabinary material blown off of the companion star by the pulsar wind (e.g. Archibald et al. 2009). In order to avoid such eclipses, we performed our GBT observations at the times when IGR J17591−2342 was close to inferior conjunction, using the ephemeris of Sanna et al. (2018) to predict orbital phase (Table 2 lists the orbital phase range of each observation). All observations were done in a high time-resolution search mode. We used the GBT *S*-band (1.73–2.60 GHz) receiver and the GUPPI recording backend in its online coherent dedispersion mode. We recorded full Stokes data over a 700-MHz (epochs 1 and 2) or 800-MHz (epoch 3) band, with 10.24 μs samples and 448 (epochs 1 and 2) or 512 (epoch 3) frequency channels of 1.56 MHz each. We used a coherent (intrachannel) dispersion measure (DM) of 250 pc cm^{-3} to compensate for the likely high DM of the source. As we discuss next, there are several pulsars associated with the Galactic bulge that have DM 177–422 pc cm^{-3}, and our coherent dedispersion trial value is in this range. The NE2001 electron density model prediction for this line of sight is 250 pc cm^{-3} at a distance of 4 kpc (Cordes & Lazio 2002). At a larger distance of 8 kpc, NE2001 predicts a DM of 635 pc cm^{-3} and a large scattering time at 2 GHz: 2.5 ms, i.e. comparable to the pulse period. For comparison, the YMW16 electron–density model predicts higher DM: 423 pc cm^{-3} for 4 kpc and 1088 pc cm^{-3} for 8 kpc. Note, however, that the scattering time-scale along any given line of sight is highly uncertain. Using the DM versus N_H relationship of He, Ng & Kaspi (2013), we find that the expected DM is in the broad range of 200−2000 pc cm^{-3}. Ultimately, the detectability of radio pulsations from IGR J17591−2342 is challenging given the likely large distance, and also depends on the scattering time-scale being favourably low compared to model predictions.

We used the PRESTO software suite (Ransom 2001; Ransom, Eikenberry & Middleditch 2002; Ransom, Cordes & Eikenberry 2003) to search the GBT data for radio pulsations. First, we

masked narrow-band and impulsive radio frequency interference (RFI) using `rfifind`. After flagging, and accounting for bandpass, the effective bandwidth of the observations is ∼550 MHz. Since the DM of IGR J17591−2342 is unknown, we must search over this parameter in order to accurately correct for dispersive delay across the observing band. We created downsampled Stokes I filterbank data with a time resolution of 81.92 µs, using `psrfits_subband`. We then produced barycentric dedispersed time series in a range from 0 to 1003.2 pc cm^{-3} using `prepsubband`, according to a dedispersion step plan calculated with `DDplan.py`. We used DM steps of 0.2, 0.3, 0.5, and 1 pc cm^{-3} and additional downsampling factors of 1, 2, 4, and 8 for DM ranges 0.0–446.4, 446.4–547.2, 547.2–787.2, and 787.2–1003.2 pc cm^{-3}, respectively, producing a total of 3264 time series for each observation.

For each of these time series, the search was performed in two ways: (1) a blind Fourier-based periodicity search and (2) direct pulse-phase folding using the known ephemeris (Sanna et al. 2018). For the blind search, we used `accelsearch`, which takes into account the Doppler shift of the pulsar period due to its orbital motion. We used z = 600, to account for a linear drift in the fundamental of up to 600 Fourier bins. For the direct pulse-phase folding search, we accounted for potential stochastic orbital variability (typical of redback systems, e.g. Archibald et al. 2013) with respect to the reference ephemeris by searching over a $|\Delta T_{\rm asc}|$ < 5 s in steps of 0.1 s. This resulted in 100 folded profiles per DM. Both search strategies and the data integrity were verified using the same approach on a 1-min test scan of PSR J1802−2124, which was easily detected. The same process failed to identify a signal plausibly associated with IGR J17591−2342.

3 RESULTS

3.1 X-ray

During its first detected outburst, IGR J17591−2342 displayed a complex X-ray light curve with multiple brightness peaks resolved by *Swift*–XRT and *NICER* (Fig. 1). Furthermore, *Swift*–BAT observations show a bright peak prior to the *INTEGRAL* discovery of the source on MJD 58340 (Ducci et al. 2018). Using *NICER* data, Ray et al. (2018) demonstrated that IGR J17591−2342 was consistently in a hard state, and that it showed coherent X-ray pulsations (Sanna et al. 2018) throughout the outburst. Our measured X-ray spectra from *Swift*–XRT also indicate that IGR J17591−2342 was in a hard state for the entire span of the radio observing campaign.

Ideally, we would also calculate an average daily hardness–intensity diagram (HID, where hardness is usually defined as the ratio of hard $\gtrsim$10 keV and soft $\lesssim$10 keV fluxes and intensity as the sum of these fluxes) during the outburst, in order to provide further context to the radio measurements. However, the source faintness and crowded field preclude sufficiently precise measurements using all-sky monitors, and offer no additional useful information. Furthermore, the high absorption and relatively low source brightness also limits the utility of an HID based on *Swift*–XRT or *NICER* $\lesssim$ 10 keV data.

The X-ray flux varied by an order of magnitude during the outburst, which translates into a luminosity range $L_{\rm X} = 4 \times 10^{35-36}$ erg s^{-1} for an assumed distance of 8 kpc ($L_{\rm X} = 4\pi D^2 S$, where S is the observed flux and D is the distance to the source). We did not detect the source in *Swift*–XRT observations after MJD 58403. For the last observation (target ID: 00010804024), we derived a 3σ upper limit on the count rate of <0.02 cnt s^{-1}

using the online *Swift*–XRT data products generator. We converted this count rate upper limit into a 1–10 keV unabsorbed flux upper limit of <0.02 × 10^{-10} erg s^{-1}cm^{-2} using WEBPIMMS[6] with $N_{\rm H} = 4.4 \times 10^{22}$ cm^{-2} and assumed photon index $\Gamma = 2$.

3.2 Radio continuum

IGR J17591−2342 was detected at all five epochs of ATCA observations and at three VLA epochs (see Table 1); it was not detected during the last two VLA epochs. The measured radio flux densities, 3σ upper limits, and spectral indices are listed in Table 1. All fluxes were converted to a 5-GHz radio luminosity, assuming a flat spectral index ($\alpha = 0$, which is consistent with the average observed value) and distance of 8 kpc, using $L_{\rm R} = 4\pi\nu D^2 S_\nu$, where ν is the central frequency and S_ν is the observed flux density. We found that $L_{\rm R}$ varies throughout the outburst, by a factor of ∼5, and drops significantly (by at least factor of 3) at the end of the outburst. The source was brightest during the first three observations previously presented by Russell et al. (2018a; see Figs 1 and 2) with $L_{\rm R}$ ∼4 × 10^{29} erg s^{-1}, and it decays after MJD 58355, where its radio luminosities were sometimes significantly lower at comparable X-ray luminosity (see Fig. 2: observations 1, 3, 4, and 5 at $L_{\rm X} = 3$–4 × 10^{36} erg s^{-1}, as well as observations 2, 6, and 7 at $L_{\rm X} = 0.9$–1.5 × 10^{36} erg s^{-1}). Given the typically large errors on the spectral indices, we do not detect any clear evolution in the radio spectrum.

3.3 Radio–X-ray relation

In order to quantify the differences between IGR J17591−2342 and other LMXBs, we performed a power-law fit to the radio and X-ray luminosities for different classes of LMXBs, as well as individual sources when the number of available measurements is sufficient (>8 $L_{\rm R}$–$L_{\rm X}$ points). Using the PYTHON implementation of the Kelly (2007) linear regression algorithm LINMIX_ERR,[7] we perform a linear fit in logarithmic space, in the form used by Gallo et al. (2014, 2018):

$$\lg L_{\rm R} - \lg L_{\rm R,c} = \lg \xi + \beta \left(\lg L_{\rm X} - \lg L_{\rm X,c} \right). \qquad (1)$$

LINMIX_ERR returns fit results for three free parameters: the power-law index β, the scaling factor ξ (which, in our case, denotes scaling of the radio luminosity value of the line intercept with respect to a reference radio luminosity $L_{\rm R,c} = 5 \times 10^{28}$ erg s^{-1}, for a fixed X-ray luminosity $L_{\rm X,c} = 2 \times 10^{36}$ erg s^{-1}) and an additional parameter, σ_0, that accounts for intrinsic random (Gaussian) scatter of the luminosities around the best-fitting power law.

In order to directly compare $L_{\rm R}$–$L_{\rm X}$ data of IGR J17591−2342 with other sources, we performed the fit for only data points within the 4×10^{35} erg s^{-1} < $L_{\rm X}$ <10^{37} erg s^{-1} range. We performed separate fits for all BH–LMXBs, non-pulsing NS–LMXBs, AMXPs (both including and excluding IGR J17591−2342), as well as separate fits for the best-sampled NS–LMXBs: IGR J17591−2342, SAX J1808.4−3658, and Aql X-1. The provenance of these data is provided in the caption of Fig. 2. The inferred mean radio luminosities $\xi + L_{\rm R,c}$ and intrinsic scatters σ_0 of each sample are presented in Fig. 3. For IGR J17591−2342, we find a best-fitting power-law slope $\beta = 0.37^{+0.42}_{-0.40}$ (Fig. 2).
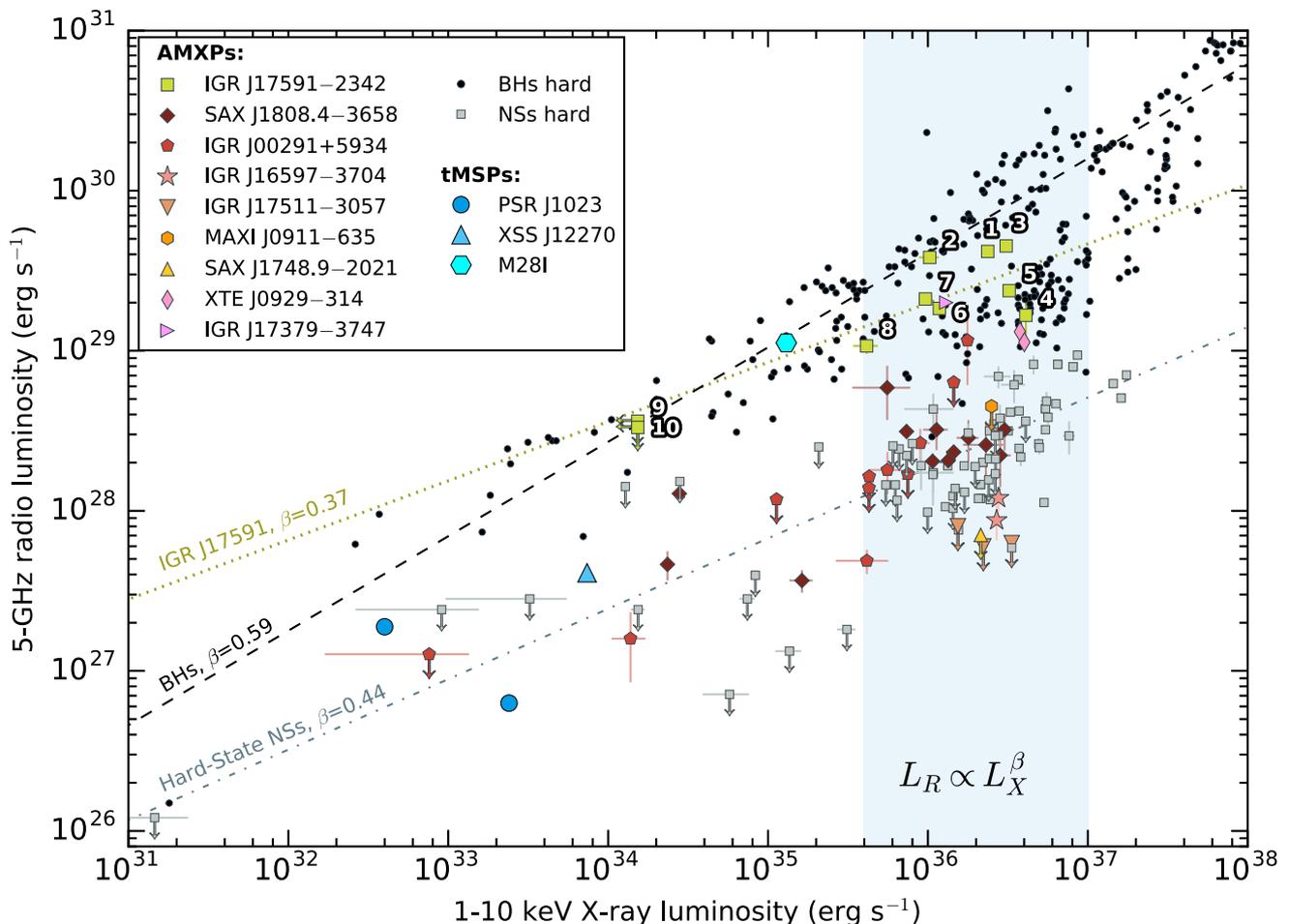
Figure 2. X-ray (1–10 keV) luminosity versus radio (5 GHz) luminosity for BH–LMXB and NS–LMXB. The black circles represent BH–LMXBs; the grey squares represent non-pulsing NS–LMXBs; a variety of symbol types and colours are used to represent individual AMXP and confirmed tMSP systems. Radio–X-ray measurements of IGR J17591−2342 are shown using the yellow–green squares (where the assumed distance is 8 kpc; see Russell et al. 2018a fig. 2, which plots the measurements for the first three epochs for a range of distances) and each observation (Table 1) is labelled with its corresponding ID number. Data points are taken from Bahramian et al. (2018) for BHs hard, Migliari & Fender (2006), Tetarenko et al. (2016), Gusinskaia et al. (2017, 2019) for NSs hard, Papitto et al. (2013), and updated X-ray value from Coti Zelati et al. (2019) for M28I, where strictly simultaneous data were used and a time-resolved X-ray spectral analysis was performed; Hill et al. (2011) for XSS J12270−4859; Bogdanov et al. (2018) for PSR J1023 + 0038; Tudor et al. (2017) for SAX J1808.4−3658, IGR J00291−5934, and IGR J17511−3057; Tetarenko et al. (2018) for IGR J16597−3704, Tudor et al. (2016) for MAXI J0911–635; Miller-Jones et al. (2010), Tetarenko et al. (2017) for SAX J1748.9−2021; Migliari, Miller-Jones & Russell (2011) for XTE J0929−314; van den Eijnden et al. (2018b) for IGR J17379−3747; Russell et al. (2018a) and this work for IGR J17591−2342. Correlation tracks for hard state BHs (the dashed black line) and NSs (the dash–dotted grey line) are defined in Gallo et al. (2018). The yellow–green dotted line represents the result of our $L_R \propto L_X{}^\beta$ fit for IGR J17591−2342. The blue-shaded area represents the $L_X = 4 \times 10^{35} - 1 \times 10^{37}$ erg s^{-1} X-ray luminosity range that we used for our comparison analysis (Fig. 3).

3.4 Radio pulsations search

In our GBT observations, we found no evidence for radio pulsations from IGR J17591−2342 during quiescence. Using the observational parameters, along with the modified radiometer equation (Dewey et al. 1985), we calculate an upper limit on the period-averaged flux density of radio pulsations. We assume a telescope gain $G = 2.0$ K Jy^{-1}, system temperature $T_{sys} = 30$ K, integration time $T = 2500$ s, effective bandwidth $B = 550$ MHz, pulse duty cycle 10 per cent, and a minimal S/N $= 8$ for a plausible detection (this is set to be relatively low because the pulse frequency is known). The resulting flux density limit is 26 μJy. This does not account, however, for intrachannel dispersive smearing at DMs far from 250 pc cm^{-3}, nor does it account for possible temporal broadening from scattering.

4 DISCUSSION

Next to SAX J1808.4−3658 and Aql X-1, IGR J17591−2342 is the best-sampled NS–LMXB in the $L_X = 4 \times 10^{35} - 1 \times 10^{37}$ luminosity range that is typically seen during the hard state of NS–LMXB accretion outbursts (see Tudor et al. 2017; Gusinskaia et al. 2019, for a discussion of these sources). IGR J17591−2342 is an AMXP (Sanna et al. 2018), with spin rate, orbital period, and companion mass similar to those of, e.g. AMXPs Swift J1749.4−2807 and SAX J1748.9−2021, as well as the established tMSPs PSR J1023 + 0038, PSR J1824−2452I and PSR J1227−4853 (see e.g. table 1 of Campana & Di Salvo 2018).

The multipeaked X-ray light curve of the outburst is not unprecedented for an LMXB – see e.g. Marino et al. (2019) for a compendium of AMXP outburst references. The persistence
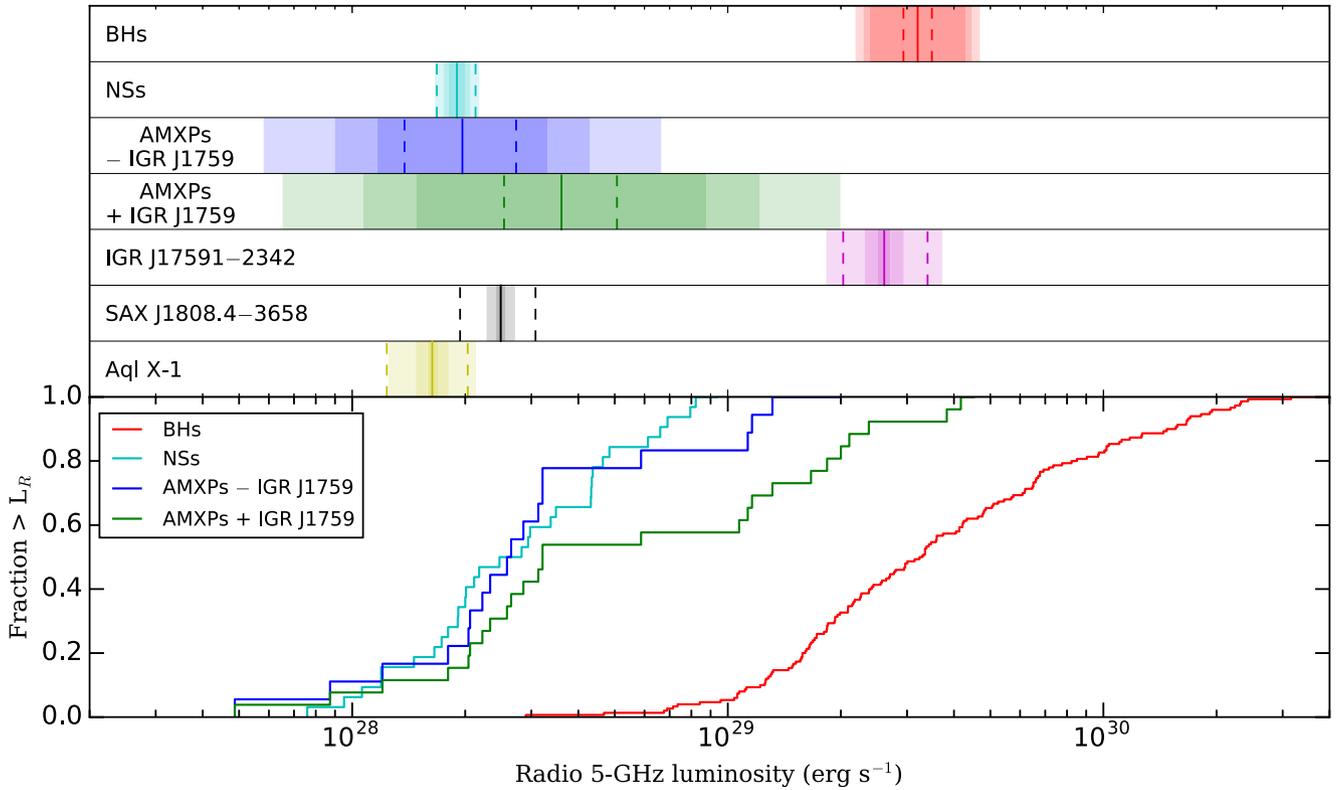
Figure 3. *Top:* Inferred parameters of the LINMIX_ERR fit (equation 1) to X-ray and radio luminosities of different classes of NS–LMXB and BH–LMXB, as well as individual sources (using an X-ray luminosity range $4 \times 10^{35}\,\mathrm{erg\,s^{-1}} < L_X < 10^{37}\,\mathrm{erg\,s^{-1}}$). The solid and dashed lines represent values of the radio luminosity intercept $\xi + L_{R,c}$ and its uncertainties, respectively. The shaded areas represent the intrinsic scatter σ_0 of radio luminosities around the best-fitting function of the slope, along with its uncertainties. *Bottom:* Cumulative distribution function for 5-GHz radio luminosities of different classes of NS–LMXB and BH–LMXB.

of coherent X-ray pulsations (Sanna et al. 2018) throughout the outburst (Ray et al. 2018) is seen in most AMXPs (Patruno & Watts 2012) with a few exceptions (Aql X-1; Casella et al. 2008, HETE J1900−2455; Patruno et al. 2017, and SAX J1748.9−2021; Altamirano et al. 2008). The fact that IGR J17591−2342 remained in the hard state, and did not transition to the soft state during the outburst is also commonly observed in AMXPs (Patruno & Watts 2012; Campana & Di Salvo 2018). In fact, IGR J17591−2342's most exceptional quality, at least for the purposes of this discussion, is its high radio luminosity during outburst.

Given the large distance to IGR J17591−2342, the lack of detected radio pulsations subsequent to the outburst is arguably unsurprising, and does not rule out an active radio pulsar during quiescence. There is no evidence that tMSPs are any fainter (or brighter) compared the rest of the known radio MSP population. Radio (millisecond) pulsars in directions a few degrees from the Galactic centre – and thus in the same general direction and potentially at a comparable distance to IGR J17591−2342 – are known (see Perera et al. 2019, who associate these with a roughly Galactic centre distance at ∼8 kpc based on their observed spin-down rates, which are dominated by acceleration in the Galactic potential). If IGR J17591−2342 was an equally bright radio pulsar compared with this sample, then we would have easily detected it in our GBT observations. Radio MSPs are generally believed to have wide beams (Lorimer & Kramer 2004), so it is unlikely that the emission cone misses the Earth. However, we cannot rule out that a large eclipse duration or temporal broadening from scattering in

the interstellar medium are responsible for the non-detection. Most AMXPs fail to show detectable radio pulsations during quiescence (e.g. Iacolina et al. 2010; Patruno et al. 2017), but this does not rule out that they become rotation-powered pulsars (e.g. Burderi et al. 2003). Their rotation-powered activity during quiescence will be better probed by the future Square Kilometre Array (Keane et al. 2015), which provides a major boost in sensitivity. Higher sensitivity allows both shorter observations, which are better suited to detecting pulsations in short orbital–period system, as well as the opportunity to search at higher radio frequencies where eclipsing is less prominent.

4.1 Radio–X-ray relation

While it is unclear whether NS–LMXBs show a single power-law relation between radio and X-ray luminosities, we none the less fit for such a correlation so that IGR J17591−2342 can be better compared with previously studied systems.

We performed the power-law fit of our L_R–L_X measurements of IGR J17591−2342 restricting to the X-ray luminosity range $4 \times 10^{35}\,\mathrm{erg\,s^{-1}} < L_X < 10^{37}\,\mathrm{erg\,s^{-1}}$ (Fig. 2) because (1) this range corresponds to that commonly seen in the hard state of NS–LMXBs in outburst and contains the highest density of archival measurements for comparison and (2) it lowers the chance of mixing different accretion physics (e.g. where a pulsar wind or propellering might have a strong effect), likely occurring at lower X-ray luminosities (e.g. Tudor et al. 2017; Bogdanov et al. 2018; Gusinskaia

et al. 2019). None the less, extending the X-ray luminosity range to lower L_X would not have a large effect on the measured slopes presented here.

For IGR J17591−2342, we find a best-fitting power-law slope $\beta = 0.37^{+0.42}_{-0.40}$ within the X-ray luminosity range 4×10^{35} erg s^{-1} $< L_X < 10^{37}$ erg s^{-1} (which does not include upper limits, i.e. epochs 9 and 10; see Fig. 2). This is consistent with the global fit to hard state NS–LMXBs found by Gallo et al. (2018), but the uncertainty on the fit is large because of the significant scatter in the measurements: $\sigma_0 = 0.05^{+0.1}_{-0.04}$ dex. Sampling IGR J17591−2342 using strictly simultaneous radio–X-ray observations would have better constrained or ruled out any L_R–L_X correlation.

Given its likely >6 kpc distance, IGR J17591−2342 is the radio-brightest AMXP detected thus far. It is consistent within the scatter with the population of BH–LMXBs (Figs 2 and 3). This underscores the importance of using more than just radio brightness in order to classify new X-ray transients as NSs or BHs.

Alternatively, the distance to IGR J17591−2342 would have to be surprisingly lower than modelled (<6 kpc; Nowak et al. 2019) to bring it more in line with the measured radio luminosities of other NS–LMXBs. However, this would introduce new questions because the large N_H would have to be ascribed to a local origin (which was deemed unlikely by Nowak et al. 2019), and the outburst would be atypically X-ray faint.

SAX J1808.4−3658 is the only other non-intermittent AMXP with comparable L_R–L_X sampling; we find that IGR J17591−2342 is a factor of 13 times more radio luminous in the 4×10^{35} erg s^{-1} $< L_X < 10^{37}$ erg s^{-1} range (Fig. 3). It is also 16 times more luminous compared to the normally non-pulsing[8] Aql X-1.

AMXPs show a very large spread in radio luminosities in the considered X-ray region (4×10^{35} erg s^{-1} $< L_X < 10^{37}$ erg s^{-1}): among them are the faintest and the brightest NS–LMXBs. Almost as luminous as IGR J17591−2342 are IGR J17379−3747, XTE J0929–314, and the AMXP/tMSP M28I (also known as IGR J18245−2452). These systems have very few available L_R–L_X measurements, however, and are thus interesting targets to explore whether they can be even more luminous. Similarly, IGR J17591−2342 was first observed only 3 weeks after the start of its 2018 outburst. The pre-discovery hard X-ray light curve (Fig. 1, panel a) suggests that the source may have been the brightest in X-rays during the initial peak, and thus we could have missed its brightest radio emission as well.

Overall, we see that the inclusion of IGR J17591−2342 in a fit to all AMXPs demonstrates that these span 1.5 dex in L_R, which is a broader range compared to that observed thus far for non-pulsing NS–LMXBs. However, this could be a bias due to such systems being preferentially targeted for study. Without the inclusion of IGR J17591−2342, we find no evidence that AMXPs are systematically brighter compared to non-pulsing NS–LMXBs: Their cumulative distributions (see Fig. 3) are almost identical. This was previously found by Gallo et al. (2018), who considered this over a larger X-ray luminosity range.

Perhaps the large scatter of radio luminosities of AMXPs in the investigated L_X range is not surprising, given their range of NS properties like spin rate, magnetic field strength, etc. Even the presumably less complex BH–LMXBs show divergent radio behaviour in the same L_X range, although with smaller scatter (~ 0.15 dex).

None the less, we see no clear reason why IGR J17591−2342 and a few other AMXPs are significantly brighter compared to the average brightness of AMXPs and non-pulsing NS–LMXBs. Tetarenko et al. (2018) investigated the influence of orbital period in ultracompact NS–LMXBs on radio brightness, but found no correlation. Similarly, Migliari et al. (2011) found no correlation between NS spin rate and radio brightness, and Russell et al. (2018a) suggested that the spin did not account for the high radio luminosity of IGR J17591−2342. Indeed, we find there is no clear difference in the spin rates of 'radio-luminous' AMXPs (IGR J17591−2342, IGR J17379−3747, XTE J0929–314, and M28I) and the rest of the population. van den Eijnden et al. (2018a) on the other hand discovered that a highly magnetized NS binary system has significantly lower radio luminosity in comparison with the less magnetized Z-type NSs, accreting at the same X-ray luminosity. Thus, the NS magnetic field strength or its inclination with respect to the accretion disc provide an interesting avenue for further investigation (e.g. Parfrey et al. 2017; Parfrey & Tchekhovskoy 2017). That said, Sanna et al. (2018) argue that IGR J17591−2342 has a typical magnetic field strength for an AMXP, which would argue against the bright radio emission being driven by a low magnetic field in this system.

Another possibility is that orbital inclination may lead to different observed radio luminosities, e.g. if the system is face-on and the jet pointed towards the observer, the expected Doppler boosting may be responsible for the high radio luminosities of some AMXPs (e.g. Russell et al. 2015). Highly beamed systems should be rare, however. Furthermore, at least in the case of IGR J17591−2342, the detection of high-velocity winds (Nowak et al. 2019) suggests that the system is closer to being seen edge-on (Higginbottom et al. 2019), arguing against such a scenario. We do note that the jet and disc from these systems may be misaligned (e.g. Maccarone 2002; Miller-Jones et al. 2019); however, this would still not adequately explain the radio emission from IGR J17591−2342.

Alternatively, the X-ray wind itself could be responsible for boosting radio luminosity via wind–jet interaction. This was previously suggested as a possible explanation for the observed radio flares in SAX J1808.4−3658 (Tudor et al. 2017). Such a scenario could also be a potential explanation for the large variability of the radio emission of IGR J17591−2342, which appears to be the brightest during the first three radio epochs. Nowak et al. (2019) found winds using a *Chandra* observation that was performed 2 d before the third and brightest ATCA observation. This remains a tentative possibility since only one high-spectral resolution observation was performed during the 2018 outburst of IGR J17591−2342; thus, the direct influence of X-ray winds on radio brightness could not be further explored.

Despite its large distance, IGR J17591−2342's radio brightness makes it a good candidate for future coordinated radio–X-ray campaigns, assuming it again goes into outburst and that the onset of the outburst is detected promptly. Because the VLA was unfortunately in its low-resolution D-array configuration, the sensitivity of these observations was limited by significant diffuse emission in the field. Using higher resolution VLA, ATCA, or MeerKAT observations in the future, there should be enough sensitivity to investigate (anti)correlated radio–X-ray variations on minutes time-scales, if sensitive (e.g. *Chandra*) and strictly simultaneous X-ray observations can be arranged. Such observations have given important insights into the accretion regime of tMSPs in the low-luminosity accretion-disc state (Bogdanov et al. 2018), but similarly sensitive and strictly simultaneous radio–X-ray campaigns have yet to be undertaken for NS–LMXBs in full outburst – where the

---

[8] Aql X-1 showed coherent X-ray pulsations for roughly 120 s out of $\sim 10^6$ s of observations (Casella et al. 2008; Messenger & Patruno 2015).

phenomenology and physics is likely quite different. At the same time, high-cadence radio–X-ray campaigns can also be valuable even if the two wavelengths are observed only quasi-simultaneously. The radio sampling achieved in the campaign presented here missed both the pre-discovery outburst peak (MJD 58320−58325) as well as a later re-brightening around MJD 58380, which if better studied could have implications for understanding the radio–X-ray coupling. If future outbursts are also multipeaked in X-rays, then high-cadence (ideally daily) observations can also better probe whether the radio tightly tracks these X-ray variations, whether there is a lag, and whether the existence of an outflowing wind correlates with radio brightness.

ACKNOWLEDGEMENTS

REFERENCES

Alpar M. A., Cheng A. F., Ruderman M. A., Shaham J., 1982, Nature, 300, 728
Altamirano D., Casella P., Patruno A., Wijnands R., van der Klis M., 2008, ApJ, 674, L45
Archibald A. M. et al., 2009, Science, 324, 1411
Archibald A. M., Kaspi V. M., Hessels J. W. T., Stappers B., Janssen G., Lyne A., 2013, preprint (arXiv:1311.5161)
Arnaud K. A., 1996, in Jacoby G. H., Barnes J., eds, ASP Conf. Ser. Vol. 101, Astronomical Data Analysis Software and Systems V. Astron. Soc. Pac., San Fransisco, p. 17
Bahramian A. et al., 2018, Radio/X-ray correlation database for X-ray binaries
Bassa C. G. et al., 2014, MNRAS, 441, 1825
Blandford R. D., Payne D. G., 1982, MNRAS, 199, 883
Blandford R. D., Znajek R. L., 1977, MNRAS, 179, 433
Bogdanov S. et al., 2018, ApJ, 856, 54
Bozzo E., Ducci L., Ferrigno C., Savchenko V., Kuulkers E., Grinberg V., Paizis A., Sidoli L., 2018, Astron. Telegram, 11942, 1
Burderi L., Di Salvo T., D'Antona F., Robba N. R., Testa V., 2003, A&A, 404, L43
Campana S., Di Salvo T., 2018, in Rezzolla L., Pizzochero P., Jones D. I., Rea N., Vidaña I., eds, Astrophysics and Space Science Library, Vol. 457, Astrophysics and Space Science Library. Springer Nature, Switzerland, p. 149
Casella P., Altamirano D., Patruno A., Wijnands R., van der Klis M., 2008, ApJ, 674, L41
Corbel S., Coriat M., Brocksopp C., Tzioumis A. K., Fender R. P., Tomsick J. A., Buxton M. M., Bailyn C. D., 2013, MNRAS, 428, 2500
Cordes J. M., Lazio T. J. W., 2002, preprint (astro–ph/0207156)
Coti Zelati F. et al., 2019, A&A, 622, A211
Deller A. T. et al., 2015, ApJ, 809, 13
Dewey R. J., Taylor J. H., Weisberg J. M., Stokes G. H., 1985, ApJ, 294, L25
Ducci L., Kuulkers E., Grinberg V., Paizis A., Sidoli L., Bozzo E., Ferrigno C., Savchenko V., 2018, Astron. Telegram, 11941, 1
Evans P. A. et al., 2007, A&A, 469, 379
Evans P. A. et al., 2009, MNRAS, 397, 1177
Ferrigno C. et al., 2018, Astron. Telegram, 11957, 1
Gallo E., Miller B. P., Fender R., 2012, MNRAS, 423, 590
Gallo E. et al., 2014, MNRAS, 445, 290
Gallo E., Degenaar N., van den Eijnden J., 2018, MNRAS, 478, L132
Gusinskaia N. V. et al., 2017, MNRAS, 470, 1871
Gusinskaia N. V., et al., 2019, preprint (arXiv:1908.04778)
He C., Ng C. Y., Kaspi V. M., 2013, ApJ, 768, 64
Higginbottom N., Knigge C., Long K. S., Matthews J. H., Parkinson E. J., 2019, MNRAS, 484, 4635
Hill A. B. et al., 2011, MNRAS, 415, 235
Homan J., Neilsen J., Allen J. L., Chakrabarty D., Fender R., Fridriksson J. K., Remillard R. A., Schulz N., 2016, ApJ, 830, L5
Iacolina M. N., Burgay M., Burderi L., Possenti A., di Salvo T., 2010, A&A, 519, A13
Keane E., et al., 2015, Advancing Astrophysics with the Square Kilometre Array (AASKA14), Proceedings of Advancing Astrophysics with the Square Kilometre Array (AASKA14). Giardini Naxos, Italy, p. 40
Kelly B. C., 2007, ApJ, 665, 1489
Krimm H. A. et al., 2013, ApJS, 209, 14
Krimm H. A. et al., 2018, Astron. Telegram, 11981, 1
Kuiper L., Tsygankov S., Falanga M., Galloway D., Poutanen J., Mereminskiy I., 2018, Astron. Telegram, 12004, 1
Lewin W. H. G., van Paradijs J., van den Heuvel E. P. J., 1997, X-ray Binaries, Cambridge University Press, Cambridge, UK
Lorimer D. R., Kramer M., 2004, Handbook of Pulsar Astronomy, Vol. 4, Cambridge University Press, Cambridge, UK
Maccarone T. J., 2002, MNRAS, 336, 1371
Marino A. et al., 2019, A&A, 627, A125
McMullin J. P., Waters B., Schiebel D., Young W., Golap K., 2007, in Shaw R. A., Hill F., Bell D. J., eds, ASP Conf. Ser. Vol. 376, Astronomical Data Analysis Software and Systems XVI. Astron. Soc. Pac., San Fransisco, p. 127
Messenger C., Patruno A., 2015, ApJ, 806, 261
Migliari S., Fender R. P., 2006, MNRAS, 366, 79
Migliari S., Fender R. P., Rupen M., Jonker P. G., Klein-Wolt M., Hjellming R. M., van der Klis M., 2003, MNRAS, 342, L67
Migliari S., Miller-Jones J. C. A., Russell D. M., 2011, MNRAS, 415, 2407
Miller J. M. et al., 2006, ApJ, 646, 394
Miller-Jones J. C. A., Heinke C. O., Sivakoff G. R., Pooley D., Homan J., Altamirano D., 2010, Astron. Telegram, 2377, 1
Miller-Jones J. C. A. et al., 2019, Nature, 569, 374
Neilsen J., Lee J. C., 2009, Nature, 458, 481
Nowak M., Paizis A., Chenevez J., Chaty S., Wilms J., Rodriguez J., 2018, Astron. Telegram, 11988, 1

Nowak M. A., Paizis A., Jaisawal G. K., Chenevez J., Chaty S., Fortin F., Rodriguez J., Wilms J., 2019, ApJ, 874, 69

Papitto A. et al., 2013, Nature, 501, 517

Papitto A. et al., 2019, ApJ, 882, 104

Parfrey K., Tchekhovskoy A., 2017, ApJ, 851, L34

Parfrey K., Spitkovsky A., Beloborodov A. M., 2016, ApJ, 822, 33

Parfrey K., Spitkovsky A., Beloborodov A. M., 2017, MNRAS, 469, 3656

Patruno A., Watts A. L., 2012, preprint (arXiv:1206.2727)

Patruno A. et al., 2017, ApJ, 841, 98

Perera B. B. P. et al., 2019, MNRAS, 487, 1025

Pinto C., Costantini E., Fabian A. C., Kaastra J. S., in't Zand J. J. M., 2014, A&A, 563, A115

Ponti G., Fender R. P., Begelman M. C., Dunn R. J. H., Neilsen J., Coriat M., 2012, MNRAS, 422, L11

Radhakrishnan V., Srinivasan G., 1982, Current Sci., 51, 1096

Ransom S. M., 2001, PhD thesis, Harvard University

Ransom S. M., Eikenberry S. S., Middleditch J., 2002, AJ, 124, 1788

Ransom S. M., Cordes J. M., Eikenberry S. S., 2003, ApJ, 589, 911

Ray P. S. et al., 2018, Astron. Telegram, 12050, 1

Roberts M. S. E., 2013, in van Leeuwen J., ed., Proc. IAU Symp. Vol. 291, Neutron Stars and Pulsars: Challenges and Opportunities after 80 years, Proceedings of International Astronomical Union. Beijing, China, p. 127

Romano P. et al., 2006, A&A, 456, 917

Russell D. M., Lewis F., 2018, Astron. Telegram, 11946, 1

Russell T. D. et al., 2015, MNRAS, 450, 1745

Russell T. D., Degenaar N., Wijnands R., van den Eijnden J., Gusinskaia N. V., Hessels J. W. T., Miller-Jones J. C. A., 2018a, ApJ, 869, L16

Russell T., Degenaar N., Wijnands R., van den Eijnden J., 2018b, Astron. Telegram, 11954, 1

Sanchez-Fernandez C., Ferrigno C., Chenevez J., Kuulkers E., Wijnands R., Bazzano A., Jonker P., Del Santo M., 2018, Astron. Telegram, 12000, 1

Sanna A. et al., 2018, A&A, 617, L8

Shaw A. W., Degenaar N., Heinke C. O., 2018, Astron. Telegram, 11970, 1

Stappers B. W. et al., 2014, ApJ, 790, 39

Tetarenko A. J. et al., 2016, MNRAS, 460, 345

Tetarenko A. J. et al., 2017, Astron. Telegram, 10843, 1

Tetarenko A. J. et al., 2018, ApJ, 854, 125

Tudor V. et al., 2016, Astron. Telegram, 8914, 1

Tudor V. et al., 2017, MNRAS, 470, 324

Tudose V., Fender R. P., Linares M., Maitra D., van der Klis M., 2009, MNRAS, 400, 2111

van den Eijnden J., Degenaar N., Russell T. D., Wijnands R., Miller-Jones J. C. A., Sivakoff G. R., Hernández Santisteban J. V., 2018a, Nature, 562, 233

van den Eijnden J. et al., 2018b, Astron. Telegram, 11487, 1

Wijnands R., van der Klis M., 1998, Nature, 394, 344

This paper has been typeset from a TeX/LaTeX file prepared by the author.